# Helium scattering structure analyses of the $c(2\times8)$ reconstruction and the high-temperature $(1\times1)$ structures of Ge(111)

D. Farías
*Institut für Experimentalphysik, Freie Universität Berlin, Arnimallee 14, 14195 Berlin, Germany*

G. Lange
*Max-Planck-Institut für Strömungsforschung, Bunsenstrasse 10, 37073 Göttingen, Germany*

K. H. Rieder
*Institut für Experimentalphysik, Freie Universität Berlin, Arnimallee 14, 14195 Berlin, Germany*

J. P. Toennies
*Max-Planck-Institut für Strömungsforschung, Bunsenstrasse 10, 37073 Göttingen, Germany*

(Received 8 July 1996)

We present a quantitative analysis of high-resolution helium-atom scattering measurements obtained from the Ge(111)-$c(2\times8)$ surface. The presence of quarter-order beams as well as the symmetries observed along $[11\bar{2}]$ and $[2\bar{1}1]$ confirm that the angular distributions are originated by three equivalent $c(2\times8)$ domains. The corrugation function derived from the calculations reveals clearly that the two rest atoms within the unit cell are buckled, as was also observed previously with scanning tunneling microscopy. Intensity analyses of diffraction scans measured above and below the order-order transition at $T_c=1050$ K suggest that for $T>T_c$ the first-layer atoms are shifted from their regular bulk places to the hexagonal diamond sites. [S0163-1829(97)01811-0]

## I. INTRODUCTION

The determination of the stable room–temperature structure of Ge(111) has been the subject of many experimental efforts in recent years. An initial attempt to characterize this structure was made by Palmberg and Peria[1] in 1967; they suggested that the simplest interpretation of the complex low-energy electron diffraction (LEED) pattern was a surface containing three domains of a $2\times8$ reconstruction, where some eighth-order spots should be structure factor forbidden. Somewhat later, Chadi and Chiang[2] proposed that the absence of the eighth-order beams occurs naturally for a $c(2\times8)$ structure, which would only require the quarter-order beams to be structure factor forbidden. This model was also supported by Yang and Jona[3] on the basis of a theoretical analysis of missing reflections. Phaneuf and Webb[4] showed that actually there are very small quarter-order LEED reflections in all positions required by three domains of a $c(2\times8)$ reconstruction, suggesting some small distortion from the basis proposed by Yang and Jona. Real-space scanning tunneling microscopy (STM) images from Ge(111)-$c(2\times8)$ were finally observed by Becker *et al.*[5] The geometrical structure was described by a simple adatom model, as shown in Fig. 1. The atoms placed at $T_4$ (top, fourfold coordinated) sites[6] are called adatoms and saturate 75% of the surface dangling bonds, leaving 25% of the surface atoms, the so-called rest atoms, unsaturated. As can be seen in Fig. 1, the $c(2\times8)$ structure contains alternating $2\times2$ and $c(2\times4)$ subunits, which leads to different local environments for each of the two adatoms and the two rest atoms within the $c(2\times8)$ unit cell. Following the notation introduced in Ref. 7, we label the four different dangling-bond states $A_3$, $A_4$, $R_3$, and $R_4$, where $A$ and $R$ stand for adatom and rest atom, respectively, and the indices refer to the sum of nearest and next-nearest dangling bonds. The fact that in the STM study of Becker *et al.* either the adatom or the rest atom was imaged, but not both simultaneously, leads to the conclusion that there is a complete electron transfer from the adatom to the rest atom, resulting in a fully occupied rest atom dangling-bond state and a completely empty adatom dangling-bond state. In a more recent STM study,

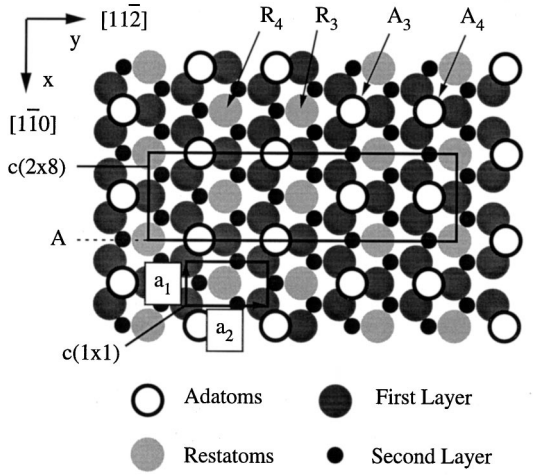


FIG. 1. Top view of the adatom model for the Ge(111)-$c(2\times8)$ reconstruction. See the text for details about the notation used in describing the two types of adatoms and rest atoms. The rectangular unit cells used in the calculations are also displayed.

 

Hirschorn *et al.*[8] could observe both rest atom and adatom dangling bonds simultaneously, which demonstrated that both kinds of dangling bonds are partially filled. Furthermore, they found that the two adatoms or the two rest atoms in a unit cell show significant differences in apparent height depending on the image conditions, the effect being more pronounced for the rest atoms than for the adatoms. This buckling may reflect a geometrical inequivalence between both adatoms (rest atoms) as well as an asymmetric distribution of the surface electronic-state density. In agreement with these results, *ab initio* calculations performed by Takeuchi *et al.*[9] showed that there is a small excess electron charge near the $R_3$-type rest atom relative to $R_4$, while no similar effect was seen for the adatoms.

In this work we present a quantitative analysis of high-resolution helium-atom scattering (HAS) data from the Ge(111)-$c(2\times8)$ surface and the high-temperature order-order transition at $T_c = 1050$ K. The study of the $c(2\times8)$ reconstruction was partly motivated by the work of Hirschorn *et al.*[8] Because of the great sensitivity of HAS to the total electron density distribution on the surface, it is interesting to ask if the asymmetries observed with STM could also be detected by means of He scattering. On the other hand, the calculations were also stimulated by the general lack of quantitative surface-structural determinations of strongly reconstructed semiconductors by means of helium-atom scattering, as compared to the wealth of work performed for metal surfaces. We will show that, despite the large unit cell, the appreciable corrugation amplitude and the complexity added by the presence of three domains, calculations performed within the simple hard-corrugated-wall (HCW) model reflect all structural details of the $c(2\times8)$ reconstruction. The sensitivity of He diffraction to the buckling observed between both rest atoms is demonstrated by model calculations performed with the eikonal approximation and the $RR'$ method within the HCW picture, on the one hand, and the close-coupled-channel method with a realistic potential, on the other hand. A similar structural analysis performed on the $1\times1$ structure, which appears above the recently reported order-order transition at $T_c = 1050$ K (Ref. 10), reveals that, in addition to the delocalization of adatoms, which occurs at $T_c$, an important rearrangement of the top-layer atoms takes place, by which they move from their normal bulk positions to sites in the hexagonal diamond lattice.

## II. EXPERIMENT

The helium-atom scattering apparatus has been described in detail in several previous reports.[11–13] Briefly, a highly monoenergetic helium-atom beam with a velocity spread of $\Delta v/v < 1\%$ is produced in a supersonic expansion and directed toward the crystal at an angle $\theta_i$ with respect to the normal. The scattered atoms are detected by a mass spectrometer, which is located at the end of a 1.43-m flight tube with the angle between incoming and outgoing beams fixed at 90°. Different momentum transfers $\Delta K$ parallel to the surface are probed by rotating the sample around an axis normal to the scattering plane, thereby accessing different incident scattering angles $\theta_i$ and final angles $\theta_f$. The present experimental diffraction patterns were performed with incident wave vectors $k_i$ of 5.5 Å$^{-1}$, 6.6 Å$^{-1}$, 7.8 Å$^{-1}$, and 9.0 Å$^{-1}$ (corresponding to $\lambda = 1.14$ Å, 0.95 Å, 0.81 Å, and 0.69 Å, respectively) at $T_s = 300$ K and in the temperature range from 940 K to 1160 K. In the high-temperature region the angular distributions are dominated by inelastic contributions because of multiphonon vibrations. Therefore the elastic signal has been extracted from the total intensity by means of time-of-flight technique as described in Ref. 10.

The Ge(111) crystal[14] ($n$-type, Sb-doped, 1.3 Ω cm, 11.5 × 5.0 × 0.25 mm$^3$; commercially grown, cut, and polished; offcut $0.2° \pm 0.1°$) was mounted between two Ta clips attached onto an *xyz* manipulator with provisions for sample tilt and azimuthal as well as polar rotations. The surface was prepared *in situ* by cycles of Ar-ion bombardment (1-keV ions, $5.7\times10^{11}$ Ar$^+$ ions/mm$^2$ s, normal incidence) for 2 h at 300 K followed by a 1-h annealing (resistively heated) at 1065 K until the Auger signal indicated a clean surface. The surface temperature was measured to within ± 5 K by an external optical pyrometer that was calibrated by melting the crystal after the experiments. The base pressure of the chamber was less than $2\times10^{-10}$ mbar with the target at 300 K, but rose as high as $5\times10^{-10}$ mbar with the target at 1100 K.

## III. DATA EVALUATION

In order to simplify the computational calculations, all the results presented in this work were obtained by using rectangular centered unit cells instead of the primitive ones. The corresponding unit cells for the $c(2\times8)$ and the $1\times1$ structures are illustrated in Fig. 1. For the sake of consistency, the indices used in the spectra refer also to the rectangular $1\times1$ unit cell.

### A. The $c(2\times8)$ structure

The already mentioned adatom model for the $c(2\times8)$ surface is illustrated in Fig. 1, whereas the reciprocal space pattern for one domain is illustrated in Fig. 2(a). The other two possible domain orientations, rotated by 120° and 240°, give rise to the complex pattern shown in Fig. 2(b). The correct identification of the contributions from the three different domains (which we label $D_1$, $D_2$, and $D_3$) in the diffraction spectra is an essential point in order to perform a reliable data analysis, as will become apparent. With this purpose, the different origins of the spots $(j,l)_i$ displayed in Fig. 2(b) are indicated by the suffix $i$, which refers to the domain $D_i$ ($i=1,2,3$) that originates the beam $(j,l)$. Note that along the symmetry directions $[112]$ and $[2\bar{1}1]$ the integer-order spots are built up by the superposition of contributions from the three domains, whereas the half- and quarter-order beams arise from just one domain. This means that the spectra measured along one of these directions already contain the two-dimensional (2D) information present in the $c(2\times8)$ unit cell, so that in principle the analysis of just one spectrum is sufficient for recovering the 2D corrugation function. Angular distributions along these directions as well as for the $[\bar{1}10]$ are shown in Fig. 3. These measurements were taken with a large He wavelength ($\lambda = 0.95$ Å) in order to obtain optimum angular resolution. As expected from the mirror symmetry present in the unit cell, the distributions along $[\bar{1}10]$ are symmetric about the specular beam

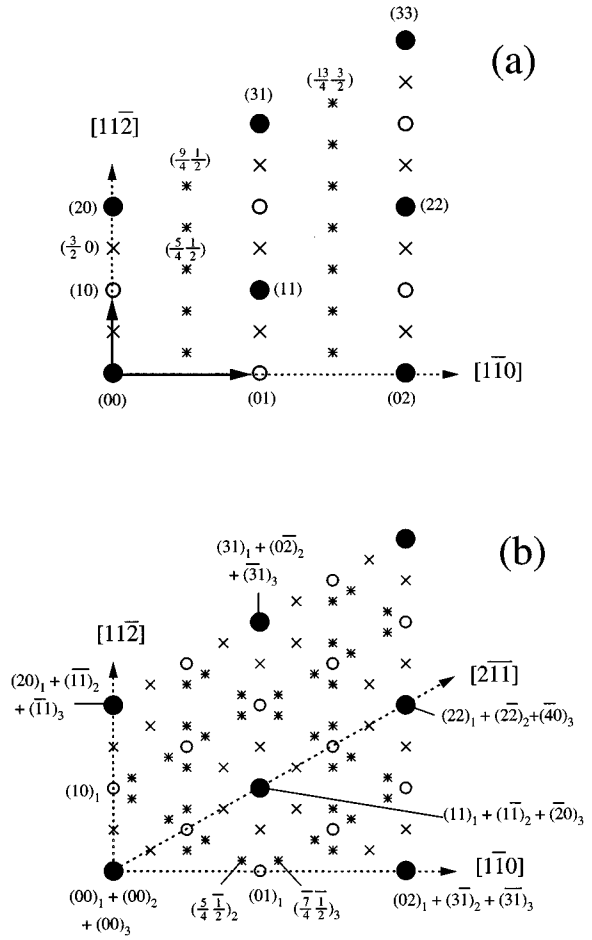


FIG. 2. (a) Reciprocal unit mesh for one domain of the Ge(111)-$c(2\times8)$ reconstruction. (b) Pattern originated by three $c(2\times8)$ domains where the notation $(j,l)_i$ indicates that the beam $(j,l)$ is originated by the domain $D_i(i=1,2,3)$. The pattern displayed in (a) is defined as $D_1$, while $D_2$ and $D_3$ were obtained by clockwise rotations of 120° and 240°, respectively.

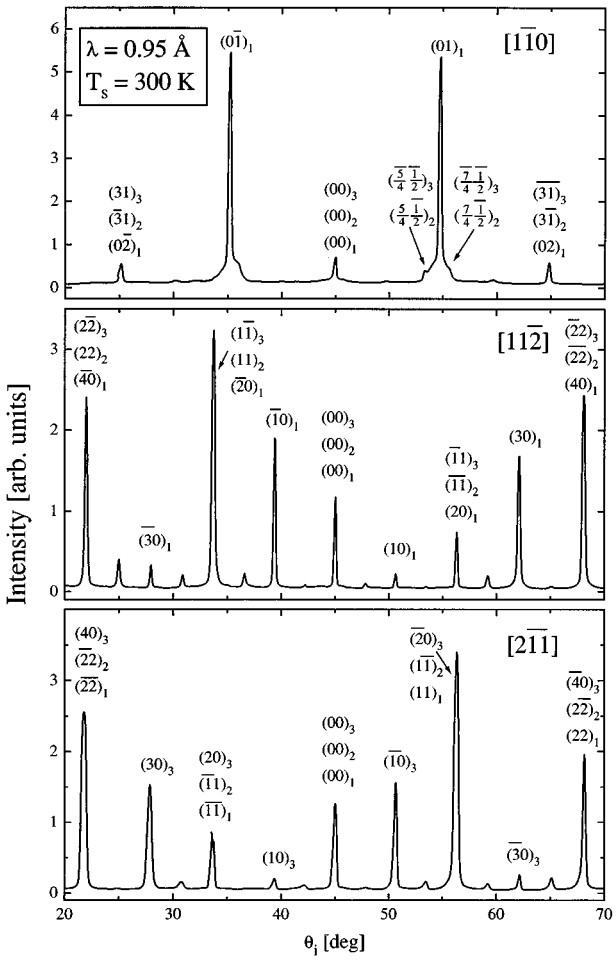


FIG. 3. Angular scans of He scattered from Ge(111) at room temperature along three principal directions. The different contributions to the integral-order beams are indicated. The indices refer to the rectangular unit cell shown in Fig. 1.

($\theta_i=45°$), implying that $I(n,m)=I(\bar{n},m)$. The scans along [11$\bar{2}$] were found to be mirror images of the ones taken along [2$\bar{1}$1], this being a consequence of the threefold symmetry of the surface. Again, the different contributions to the integral-order beams are indicated.

Whereas it seems reasonable to assume that the three domains are equally distributed on the surface, a more detailed look into these spectra provides experimental support to this question. In effect, from the fact that the relative intensities of integer- and half-quarter-order beams are the same along [112] and [2$\bar{1}$1] we can conclude that the surfaces covered by domains $D_1$ and $D_2$ are essentially the same. Unfortunately, due to the experimental limitations of our manipulator we could not measure spectra for $\phi=120°$ and therefore we are not able to estimate the proportion of $D_3$ domains present on the surface, though it seems improbable that it differs from the other two. With respect to the presence of $2\times2$ and $c(2\times4)$ unit cells, it is known from STM studies[7,8] that they do not extend over large regions and are usually observed in the form of small patches, located near the boundary between two different $c(2\times8)$ regions. With this observation in mind, we assume that all diffraction patterns originate from three equivalent domains, each corresponding to a $c(2\times8)$ structure.

Analyses of beam intensities to obtain the best-fit corrugations were, in a first step, performed with use of the eikonal approximation within the HCW model.[15] This approximation is known to yield reliable intensities only in the limit of weak corrugations (less than 10% of the lattice constant) and angles of incidence smaller than 40°. As a consequence of the experimental setup used, the angle of incidence is continuously changed from 15° to 75° during a measurement, making a comparison with exact HCW calculations necessary, as discussed below. Though the geometrical arrangement of adatoms/rest atoms in the $c(2\times8)$ unit cell seems to have been reliably established in the earlier STM studies,[5–8] we prefer to derive the corrugation function from our experimental data without any assumptions on the structure. For this purpose, we begin by choosing the most general Fourier representation for the corrugation function compatible with the mirror symmetry present along [112] (the notation refers to the rectangular $c(2\times8)$ unit cell shown in Fig. 1, with the $x$ axis along [110]), which reads

$$\zeta(x,y)=\mathcal{F}\sum_{m,n\geq 0} c_{mn}[a_{mn}\cos(mX)\cos(nY) + b_{mn}\cos(mX)\sin(nY)], \quad (1)$$

with

$$c_{mn}=\begin{cases} 0, & m+n \text{ odd} \\ \frac{1}{4}, & m \text{ or } n=0 \\ \frac{1}{2}, & \text{otherwise,} \end{cases}$$

where $X=x(2\pi/b_1)$, $Y=y(2\pi/b_2)$, with $b_1=2a_1$ and $b_2=4a_2$ ($a_1=4.00$ Å and $a_2=4\sqrt{3}$ Å are the lattice parameters of the rectangular $1\times1$ unit cell), and $\mathcal{F}$ is a scale factor. A simple uniform attractive well of depth $D$ was added to the hard-wall repulsion, which leads to a refraction of the incident and outgoing beams. The depth $D$ was taken as an adittional fitting parameter and was allowed to vary between 0 and 12 meV in 2-meV steps. The fits were typically started with 12 different Fourier coefficients, which were varied until optimum agreement between measured $P_G^{\text{expt}}$ and calculated $P_G^{\text{calc}}$ intensities (normalized with respect to the specular beam) was achieved. This was judged computationally by means of the reliability $R$ factor

$$R=\frac{1}{N}\sqrt{\sum_G (P_G^{\text{expt}}-P_G^{\text{calc}})^2}, \quad (2)$$

where $N$ denotes the number of beams $G$ measured. Different sets of parameters were chosen every time. After many trials, the spectra could be very well fitted for two different He atom wavelengths ($\lambda=0.69$ Å and $\lambda=0.81$ Å) by taking eight Fourier coefficients ($\mathcal{F}=1$) and $D=4$ meV. The best-fit parameters for $\lambda=0.81$ Å are $a(20)=0.19$ Å, $a(02)=-0.27$ Å, $a(13)=-0.09$ Å, $a(15)=0.57$ Å, $a(24)=0.12$ Å, $b(11)=0.64$ Å, $b(13)=0.54$ Å, and $b(04)=-1.00$ Å, the $R$ factor being $R=0.051$. For $\lambda=0.69$ Å, best fits were obtained with $a(20)=0.17$ Å, $a(02)=-0.29$ Å, $a(13)=-0.16$ Å, $a(15)=0.52$ Å, $a(24)=0.09$ Å, $b(11)=0.62$ Å, $b(13)=0.52$ Å, and $b(04)=-1.10$ Å, with $R=0.068$. No other $R$-factor minima have been found in parameter space. The corresponding calculated peak intensities are shown in Fig. 4 as crosses. Although the agreement for some beams is not very good, the general trend in the intensity distributions is very well reproduced by the calculations. As a consequence, the derived corrugation function can be considered a realistic approximation for testing the validity of the eikonal theory. Our model-free analysis of the surface structure has actually reduced the number of possible corrugation functions to 2, since essentially the same intensities are obtained from $+\zeta(x,y)$ or $-\zeta(-x,-y)$ in a single scattering approach (like the eikonal approximation). In order to know which of the two functions is the correct one, it is necessary to consider the results provided by other experimental techniques and/or theoretical calculations. Results consistent with the adatom model based on the STM investigations of Becker *et al.*[5] (also supported by *ab initio* calculations[9]) were obtained for only one of the two possible corrugation functions. The corrugation profile along cut $A$ in Fig. 1 is displayed in Fig. 5, where the maxima correspond to adatoms and rest atoms following the notation introduced above.

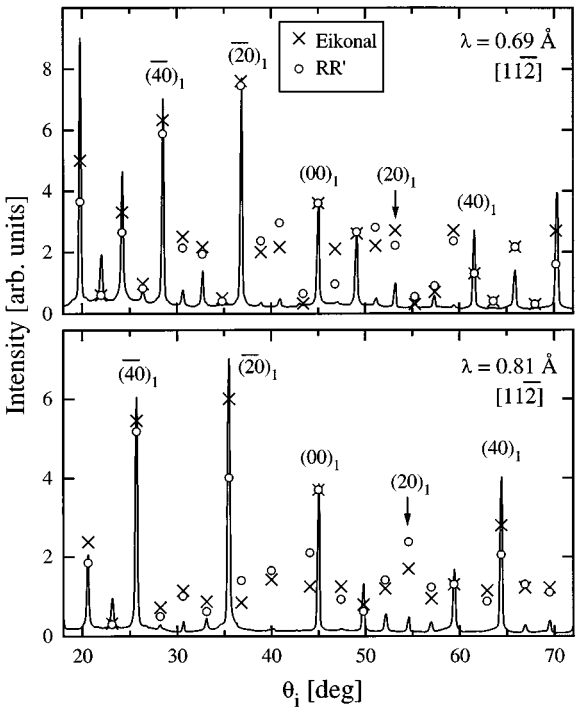


FIG. 4. Best-fit intensities calculated with eikonal ($x$) and the $RR'$ method (o) for two different He wavelengths. The corrugation function has been modeled by a Fourier ansatz [Eq. (1)].

The maximum corrugation amplitudes along $[\bar{1}10]$ and $[11\bar{2}]$ are $\zeta_X\sim1.10$ Å and $\zeta_Y\sim1.50$ Å, respectively. The first of these values represents almost 15% of the corresponding lattice constant, suggesting that the problem under consideration could be outside the range of validity of the eikonal theory. In a second step, the results were therefore checked by performing calculations with use of the $RR'$ method,[16] which represents the exact solution for a HCW interaction potential. The calculation of a unique intensity with this method requires the inversion of a matrix whose dimension $M$ depends on the magnitude of the problem under consideration [for the $c(2\times8)$ structure, $M\sim700$]; this makes the

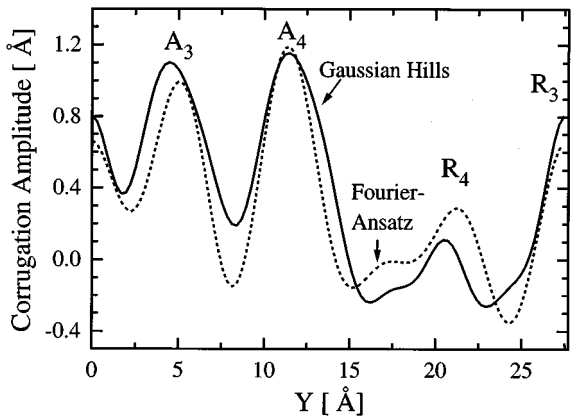


FIG. 5. Contours of the best-fit corrugations along cut $A$ in Fig. 1 derived from calculations performed with the eikonal approximation. The dashed curve corresponds to a corrugation described by a Fourier representation, while the full line was obtained by modeling the adatoms/rest atoms in the unit cell as Gaussian hills.

TABLE I. Comparison of the best-fit intensities obtained with the eikonal approximation and the $RR'$ method for the $c(2\times8)$ structure by modeling the surface with a Fourier ansatz. All calculations were performed with $D=4$ meV and $\lambda=0.81$ Å. In the case of the eikonal approximation, results derived by modeling the corrugation with Gaussian hills are also shown (see the text for further details).

| Beam | $\theta_i$ (deg) | $I_{\text{expt}}$ | $I_{\text{eiko}}^{\text{Gauss}}$ | $I_{\text{eiko}}^{\text{Fourier}}$ | $I_{RR'}^{\text{Fourier}}$ |
|---|---|---|---|---|---|
| (00) | 45.05 | 1.00 | 1.00 | 1.00 | 1.00 |
| $(\bar{\frac{1}{2}}0)$ | 42.69 | 0.00 | 0.31 | 0.34 | 0.61 |
| $(\frac{1}{2}0)$ | 47.41 | 0.01 | 0.22 | 0.32 | 0.23 |
| $(\bar{1}0)$ | 40.33 | 0.01 | 0.17 | 0.37 | 0.44 |
| (10) | 49.77 | 0.33 | 0.32 | 0.20 | 0.15 |
| $(\bar{\frac{3}{2}}0)$ | 37.96 | 0.00 | 0.17 | 0.22 | 0.36 |
| $(\frac{3}{2}0)$ | 52.14 | 0.12 | 0.01 | 0.27 | 0.31 |
| $(\bar{2}0)$ | 35.58 | 1.94 | 1.88 | 1.68 | 1.12 |
| (20) | 54.52 | 0.10 | 0.06 | 0.49 | 0.67 |
| $(\bar{\frac{5}{2}}0)$ | 33.18 | 0.08 | 0.05 | 0.22 | 0.15 |
| $(\frac{5}{2}0)$ | 56.92 | 0.07 | 0.19 | 0.21 | 0.28 |
| (30) | 30.76 | 0.07 | 0.00 | 0.31 | 0.26 |
| (30) | 59.34 | 0.42 | 0.05 | 0.42 | 0.41 |
| $(\bar{\frac{7}{2}}0)$ | 28.31 | 0.03 | 0.02 | 0.17 | 0.11 |
| $(\frac{7}{2}0)$ | 61.79 | 0.00 | 0.06 | 0.27 | 0.19 |
| (40) | 25.83 | 1.64 | 1.42 | 1.44 | 1.52 |
| (40) | 64.27 | 1.11 | 1.13 | 0.75 | 0.53 |
| $(\bar{\frac{9}{2}}0)$ | 23.32 | 0.20 | 0.02 | 0.02 | 0.01 |
| $(\frac{9}{2}0)$ | 66.78 | 0.05 | 0.09 | 0.30 | 0.32 |
| (50) | 20.76 | 0.47 | 0.10 | 0.65 | 0.45 |
| (50) | 69.34 | 0.08 | 0.49 | 0.29 | 0.26 |

use of the $RR'$ method very time consuming and consequently inappropriate for trial and error searches in parameter space. The results obtained with the $RR'$ method using the best-fit corrugation derived with the eikonal approximation are shown in Fig. 4 as open circles. The quality of the agreement is illustrated in Tables I and II, where the intensities calculated for $\lambda=0.81$ Å and $\lambda=0.69$ Å are listed. The very good agreement between both methods justifies further attempts to improve the fits by using the eikonal approximation.

Before describing the way in which such improvements were achieved, some comments on the results already presented should be made. First, the cuts shown in Fig. 5 already illustrate one of the main results of the present work, namely, the presence of a pronounced buckling between both rest atoms in the unit cell. Note that, although a difference in heights is also observed for the two adatoms, the fact that this effect is smaller by a factor of 2 does not answer the question of whether this buckling has a physical origin or is just an artifact of the calculations. Second, the discrimination between $T_4$ and $H_3$ sites for the adatoms can be unambiguously achieved from the asymmetries observed around $R_4$. It can easily be shown that the protrusion observed between $A_4$ and $R_4$ (originated by second-layer atoms) is indeed only compatible with adatoms occupying $T_4$ sites.

A natural way to improve the fits obtained with a Fourier ansatz is by taking into account the correlations between adatoms and rest atoms in the unit cell. A way to do this is to treat the different kind of atoms $A_3$, $A_4$, $R_3$, and $R_4$ as independent groups of Gaussian hills $G(x,y)$, each having amplitudes $h_{A_3}$, $h_{A_4}$, $h_{R_3}$, and $h_{R_4}$:

$$G(x,y)=\sum_i h_{A_i,R_i}\exp\left\{-4\ \ln 2\left[\left(\frac{x-x_i}{\sigma_x}\right)^2+\left(\frac{y-y_i}{\sigma_y}\right)^2\right]\right\}, \tag{3}$$

where $i$ denotes a specific adatom (rest atom) with height $h_{A_{3,4}}$ ($h_{R_{3,4}}$) located at $(x_i,y_i)$ and full widths at half maximum $\sigma_x$ and $\sigma_y$ along the $x$ and $y$ directions, respectively. The atoms were fixed at their theoretical bulk positions, i.e., $(x_i,y_i)=(0,\frac{2}{3}a_2)$, $(0,\frac{5}{3}a_2)$, $(a_1,\frac{8}{3}a_2)$, $(a_1,\frac{11}{3}a_2)$, $(2a_1,\frac{2}{3}a_2)$, and $(2a_1,\frac{5}{3}a_2)$ for the adatoms and $(x_i,y_i)=(0,0)$, $(0,3a_2)$, $(0,4a_2)$, $(a_1,a_2)$, $(a_1,2a_2)$, $(2a_1,0)$, $(2a_1,3a_2)$ and $(2a_1,2a_2)$ for the rest atoms. The corrugation originating from the first- and second-layer atoms was simulated by a Fourier series as in Eq. (1) with coefficients $a(24)=a(08)=1.00$ Å and $a(24)=-b(08)=-0.20$ Å, where the factor $\mathcal{F}$ was taken as a fit parameter. In order to reduce the number of free parameters involved in the calculations, the Gaussian hills were first assumed to be symmetric in both $x$ and $y$ directions so that $\sigma_A=\sigma_{A_x}=\sigma_{A_y}$ for the adatoms and $\sigma_R=\sigma_{R_x}=\sigma_{R_y}$ for the rest atoms. Later we tested the sensitivity of the calculated spectra to asymmetric Gaussian hills. The fits could be slightly improved by taking $\sigma_{R_x}\neq\sigma_{R_y}$ for the rest atoms, while no similar effect was observed by modeling adatoms with $\sigma_{A_x}\neq\sigma_{A_y}$. The best-fit parameters corresponding to $\lambda=0.81$ Å and $D=4$ meV are $h_{R_4}=0.15$ Å,

TABLE II. Same as Table I but for $\lambda = 0.69$ Å.

| Beam | $\theta_i$ (deg) | $I_{\text{expt}}$ | $I_{\text{eiko}}^{\text{Gauss}}$ | $I_{\text{eiko}}^{\text{Fourier}}$ | $I_{RR'}^{\text{Fourier}}$ |
|---|---|---|---|---|---|
| (00) | 45.05 | 1.00 | 1.00 | 1.00 | 1.00 |
| $(\bar{\frac{1}{2}}0)$ | 43.01 | 0.03 | 0.19 | 0.08 | 0.13 |
| $(\frac{1}{2}0)$ | 47.09 | 0.02 | 0.11 | 0.52 | 0.21 |
| (10) | 40.96 | 0.07 | 0.78 | 0.54 | 0.74 |
| $(\bar{1}0)$ | 49.14 | 0.69 | 0.58 | 0.71 | 0.71 |
| $(\bar{\frac{3}{2}}0)$ | 38.91 | 0.03 | 0.40 | 0.50 | 0.61 |
| $(\frac{3}{2}0)$ | 51.19 | 0.07 | 0.03 | 0.67 | 0.82 |
| (20) | 36.85 | 2.18 | 1.98 | 2.17 | 2.07 |
| $(\bar{2}0)$ | 53.25 | 0.25 | 0.63 | 0.74 | 0.66 |
| $(\bar{\frac{5}{2}}0)$ | 34.78 | 0.06 | 0.46 | 0.12 | 0.05 |
| $(\frac{5}{2}0)$ | 55.32 | 0.08 | 0.56 | 0.06 | 0.12 |
| (30) | 32.70 | 0.32 | 0.11 | 0.48 | 0.46 |
| $(\bar{3}0)$ | 57.40 | 0.12 | 0.34 | 0.14 | 0.19 |
| $(\bar{\frac{7}{2}}0)$ | 30.60 | 0.15 | 0.33 | 0.63 | 0.48 |
| $(\frac{7}{2}0)$ | 59.50 | 0.03 | 0.03 | 0.75 | 0.67 |
| (40) | 28.48 | 1.99 | 2.10 | 1.81 | 1.64 |
| $(\bar{4}0)$ | 61.62 | 0.77 | 0.96 | 0.36 | 0.36 |
| $(\bar{\frac{9}{2}}0)$ | 26.33 | 0.11 | 0.18 | 0.16 | 0.11 |
| $(\frac{9}{2}0)$ | 63.77 | 0.01 | 0.23 | 0.02 | 0.01 |
| (50) | 24.16 | 1.20 | 0.69 | 0.89 | 0.63 |
| $(\bar{5}0)$ | 65.94 | 0.38 | 0.26 | 0.52 | 0.49 |
| $(\bar{\frac{11}{2}}0)$ | 21.96 | 0.45 | 0.08 | 0.04 | 0.04 |
| $(\frac{11}{2}0)$ | 68.14 | 0.01 | 0.03 | 0.03 | 0.03 |
| (60) | 19.72 | 2.67 | 1.72 | 1.40 | 1.02 |
| $(\bar{6}0)$ | 70.38 | 1.20 | 1.13 | 0.48 | 0.41 |

$h_{R_3} = 0.85$ Å, $h_{A_3} = 1.40$ Å, $h_{A_4} = 1.45$ Å, $\sigma_{Ad} = 4.25$ Å, $\sigma_{R_x} = 3.40$ Å, $\sigma_{R_y} = 2.85$ Å, and $\mathcal{F} = 0.20$, with an $R$ factor $R = 0.041$. With $\lambda = 0.69$ Å and $D = 4$ meV, a minimum $R$ factor $R = 0.062$ is achieved with $h_{R_4} = 0.25$ Å, $h_{R_3} = 0.80$ Å, $h_{A_3} = 1.55$ Å, $h_{A_4} = 1.55$ Å, $\sigma_{Ad} = 4.40$ Å, $\sigma_{R_x} = 3.40$ Å, $\sigma_{R_y} = 3.20$ Å, and $\mathcal{F} = 0.10$. Calculated diffraction spectra are shown in Fig. 6 for both He-atom wavelengths. The agreement with the experimental data is improved for the same number of free parameters (8). However, examination of Fig. 5 reveals that the essential features of the corrugation had been well reproduced by the calculations based on a Fourier ansatz, though the buckling between $R_3$ and $R_4$ has now become more pronounced and the differences between $A_3$ and $A_4$ have practically vanished. This can be seen in more detail in Fig. 7, which shows a gray scale representation of the best-fit corrugation.

### B. Error-estimation tests

Although we have demonstrated that the eikonal theory is a reliable approximation for modeling the $c(2\times8)$ structure, two questions remain. The first question has to do with the minimum buckling between adatoms/rest atoms that can be detected by the calculations. The second point concerns the link between the existence of buckling and the HCW assumption, i.e., to which extent the observed asymmetries can be ascribed to a physical origin and not to the HCW approxi-

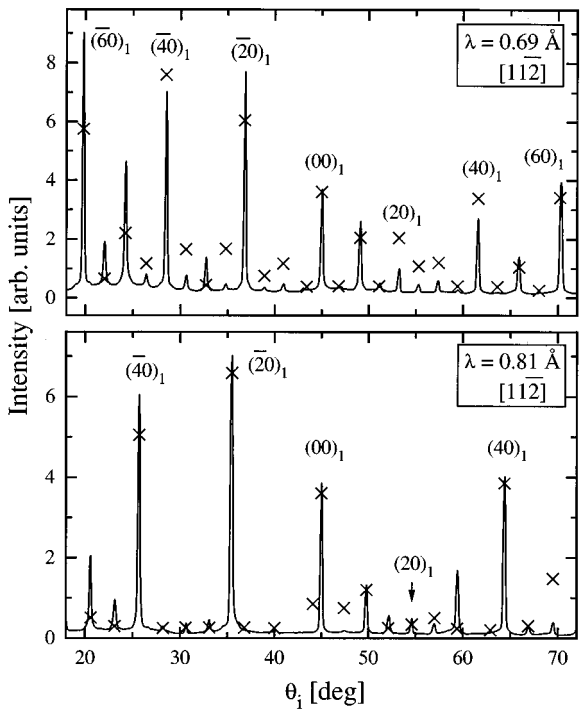


FIG. 6. Best-fit intensities calculated with eikonal (×) for two different He wavelengths. The corrugation function has been modeled by treating the different groups of adatoms/rest atoms in the unit cell as independent groups of Gaussian hills.

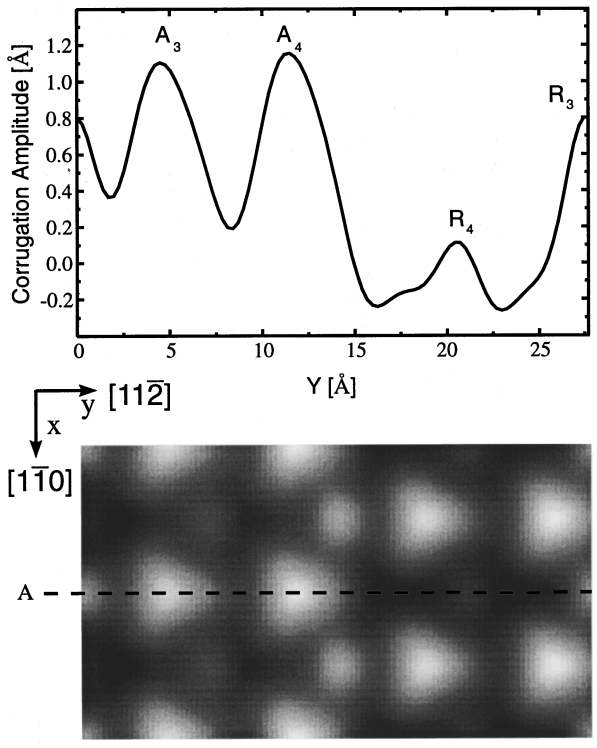


FIG. 7. Gray scale representation of the best-fit corrugation derived from the fits shown in Fig. 6 (bottom). On the top a cut along line *A* is displayed. The different types of adatoms/rest atoms in the unit cell are indicated following the notation outlined in the text.

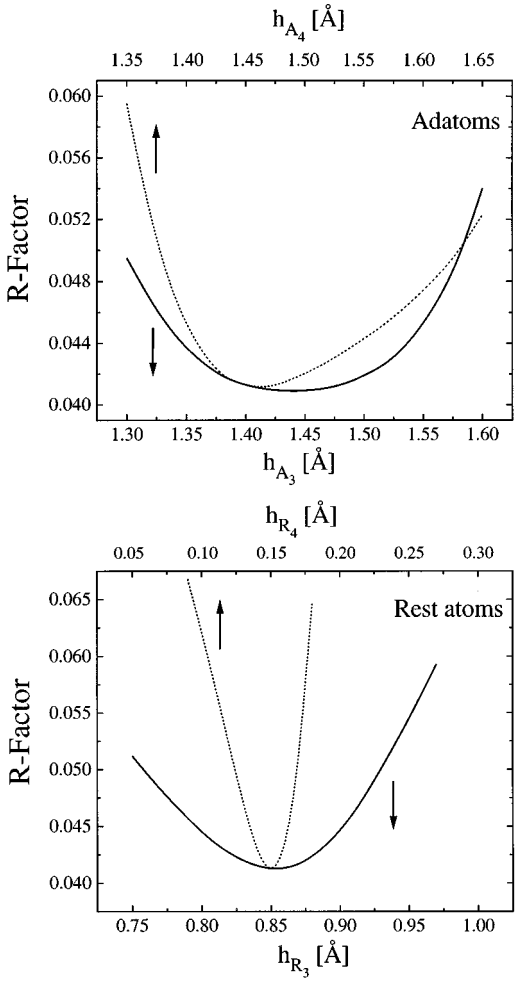


FIG. 8. Sensitivity of the $R$ factor to the four different amplitudes $h_{A_3}$, $h_{A_4}$, $h_{R_3}$, and $h_{R_4}$ used for describing the best-fit corrugation shown in Fig. 7. Only one parameter $h_i$ was varied at a time, while the others were fixed at their best-fit values.

mation. It should be clear that, when addressing these questions, we are assuming that the $R$-factor minimum has already been determined with considerable confidence. This assumption is well justified since (as discussed in Sec. III A) only one minimum was found in the fitting procedure.

In order to answer the first question, we have investigated the sensitivity of our results to the presence of a small buckling $\Delta_A = h_{A_3} - h_{A_4}$ and $\Delta_R = h_{R_3} - h_{R_4}$ between both adatoms and rest atoms, respectively. This was made by testing the dependence of the $R$ factor to the four different $h_i$'s introduced in Eq. (3). A graphical representation of this dependence is presented in Fig. 8. The calculations were performed using the corrugation function defined in Eq. (3) for $\lambda = 0.81$ Å, where only one parameter $h_i$ was varied at a time and all others were kept fixed at their best-fit values. If we define our error bars for $R$ as $\delta_R \sim 0.005$ (i.e., $\sim 10\%$ of $R$, a realistic value that can be clearly detected in the calculations) we see in Fig. 8 that $R$ is not as sensitive to $\Delta_A$ as it is to $\Delta_R$. In effect, values of $\Delta_A \sim 0.20$ Å can be obtained by requiring $\delta_R \leqslant 0.005$, while in the case of the rest atoms our worst-case predictions are reduced to $\Delta_R \sim 0.13$ Å. We take thus 0.20 Å for adatoms and 0.13 Å for rest atoms as the minimum buckling that can be detected by calculations performed within the HCW framework. This implies that the slight asymmetries observed between $A_3$ and $A_4$ in Fig. 7 cannot be attributed to a physical origin, while in the case of the rest atoms the existence of a buckling in the $c(2\times 8)$ unit cell is unambiguously correct.

We now come to the more complex question about possible links between the prediction of buckling by the calculations and the use of the HCW approximation. A more exact statement of this problem can be summarized in the two following points. (i) Can the HCW assumption turn a symmetric corrugation into an asymmetric one or vice versa? In case the answer is negative, (ii) what can be said about the influence of a realistic potential on the minimum $\Delta_A$ and $\Delta_R$ values that can be detected within the HCW approximation? Although a general answer to these questions is not trivial, we will show that for the particular case of the $c(2\times 8)$ structure there are good reasons to believe that the results presented in Sec. III A would not be seriously affected by considering the exact He-Ge(111) interaction potential in the calculations.

The approach adopted can be summarized as follows. For given asymmetric and symmetric one-dimensional corrugations, diffraction spectra were calculated by performing close-coupled-channel (CCC) calculations[17] with a realistic potential. These spectra were then fitted with the eikonal approximation using the same procedure we applied for the $c(2\times 8)$ structure. By comparing the best-fit corrugations obtained with the eikonal approximation to the ones used in the CCC calculations, the error introduced by use of the HCW approximation can be estimated.

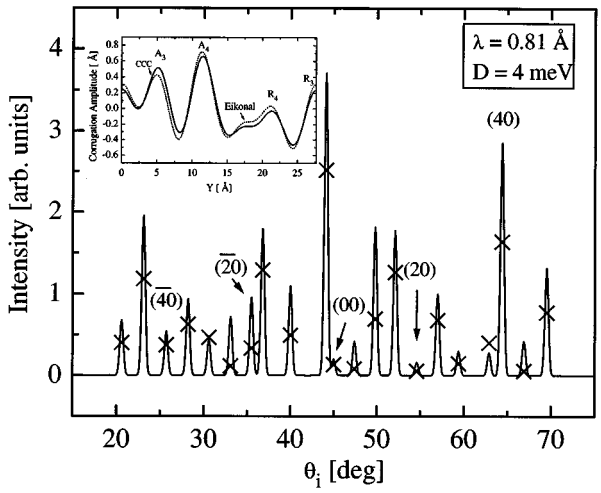


FIG. 9. Spectrum (full line) obtained by CCC calculations using a Morse potential [Eq. (4)] with $D=4$ meV and $\alpha=0.83$ Å$^{-1}$, whereas the best-fit intensities obtained with eikonal are indicated by crosses. The corrugation derived by the eikonal approximation is compared in the inset (dashed line) with the one used in the CCC calculations (full line).

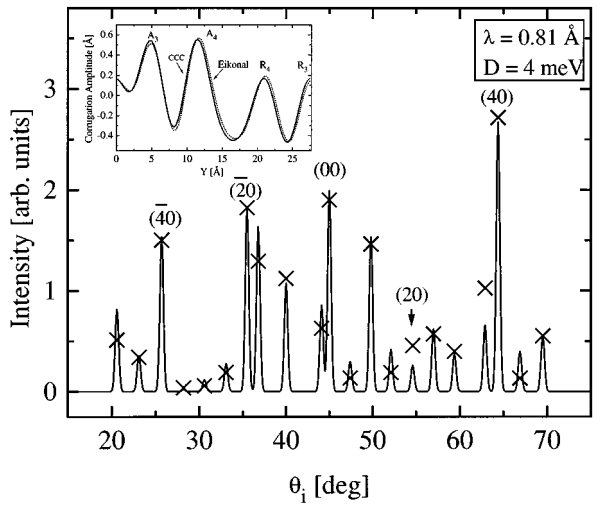


FIG. 10. Same as Fig. 9, but for a symmetric corrugation (i.e., $\Delta_A=\Delta_R=0$).

The CCC calculations were performed by using the two-parameter Morse potential

$$V(z)=D(e^{-2\alpha z}-2e^{-\alpha z}), \tag{4}$$

where $D$ is the potential well depth and $\alpha$ the range parameter. Although the exact form of the He-Ge(111) interaction potential is not known, Eq. (4) provides a realistic approximation in order to test the reliability of the HCW in structural determinations. Spectra were calculated for $\lambda=0.81$ Å and $\lambda=0.69$ Å with $D=4$ meV and $\alpha=0.83$ Å$^{-1}$. For computational simplicity, corrugation functions based on a Fourier ansatz [Eq. (2)] were used. The asymmetric function was chosen to be very similar in form to the best-fit one obtained for the $c(2\times8)$ structure, i.e., asymmetries $\Delta_A\sim0.15$ Å and $\Delta_R\sim0.30$ Å were assumed. This was made by taking the coefficients $a(02)=0.09$ Å, $a(03)=-0.07$ Å, $a(04)=0.07$ Å, $a(05)=0.40$ Å, $b(01)=0.49$ Å, $b(03)=0.40$ Å, and $b(04)=-0.37$ Å. The corresponding contour is shown as the inset in Fig. 9 (full line). Note that the maximum corrugation amplitude has been reduced to $\zeta_Y\sim1.10$ Å in order to guarantee convergence of the eikonal approximation, whose range of validity is smaller for one-dimensional than for two-dimensional problems. Calculated diffraction spectra for $\lambda=0.81$ Å are shown in Fig. 9, where they are directly compared to the best-fit intensities obtained with eikonal. Best agreement was obtained for $D=4$ meV, $a(02)=0.27$ Å, $a(03)=0.03$ Å, $a(04)=0.03$ Å, $a(05)=0.44$ Å, $b(01)=0.40$ Å, $b(03)=0.50$ Å, $b(04)=-0.74$ Å, and $b(05)=-0.04$ Å, corresponding to an $R$ factor $R=0.33$. A cut along this function is shown as the inset (dashed line) in Fig. 9. All essential features of the original corrugation are clearly reproduced, though the agreement between both calculated spectra is not especially good. A similar analysis has been performed for a symmetric corrugation (i.e., $\Delta_A=\Delta_R=0$) defined by $a(01)=0.08$ Å, $a(03)=-0.14$ Å, $a(04)=0.12$ Å, $a(05)=0.28$ Å, $b(01)=0.44$ Å, $b(03)=0.52$ Å, $b(04)=-0.37$ Å, and $b(05)=-0.13$ Å. Intensities calculated with the eikonal approximation for $\lambda=0.81$ Å and $D=4$ meV are presented in Fig. 10. The best-fit corrugation parameters are $a(01)=0.04$ Å, $a(02)=0.05$ Å, $a(03)=-0.22$ Å, $a(04)=0.16$ Å, $a(05)=0.30$ Å, $b(01)=-0.40$ Å, $b(03)=0.53$ Å, $b(04)=-0.66$ Å, and $b(05)=-0.08$ Å, the corresponding $R$ factor being $R=0.020$. A look at the inset in Fig. 10 reveals that no asymmetries are obtained with the eikonal calculation if no buckling is assumed in the CCC calculations.

These results strongly suggest that the answer to the first of the questions posed above is negative, namely, the HCW assumption is not able to turn a symmetric corrugation into an asymmetric one or vice versa. In order to determine the range of validity of this conclusion, we have investigated the sensitivity of our one-dimensional results to the presence of small bucklings $\Delta_A$ and $\Delta_R$. This was made by examinig the behavior of the $R$ factor in parameter space in a similar way as the one described above for the $c(2\times8)$ reconstruction (Fig. 8). We obtained $\Delta_A=0.15$ Å and $\Delta_R=0.09$ Å as the minimum buckling values that can be detected by the eikonal approximation for a one-dimensional corrugation. We have also looked at the effect of varying the potential used in the CCC calculations. We find no substantial differences from the results presented above for calculations performed with $D=8$ meV and $\alpha=1.20$ Å$^{-1}$. In comparing these results with the ones obtained for the $c(2\times8)$ reconstruction, two important features should be noted. First, the calculations are more sensitive to $\Delta_R$ as to $\Delta_A$ also for the one-dimensional problem. Second, the limits derived for $\Delta_A$ and $\Delta_R$ are comparable in both cases. Remember that the maximum corrugation amplitude has been reduced in the one-dimensional case. These observations suggest a quite similar behavior of both one- and two-dimensional corrugations in simulations performed within the HCW framework. In summary, we conclude that the asymmetries observed for both rest atoms in the $c(2\times8)$ unit cell cannot be a mere consequence of the eikonal approximation and must, as a consequence, be accepted as a physical effect.

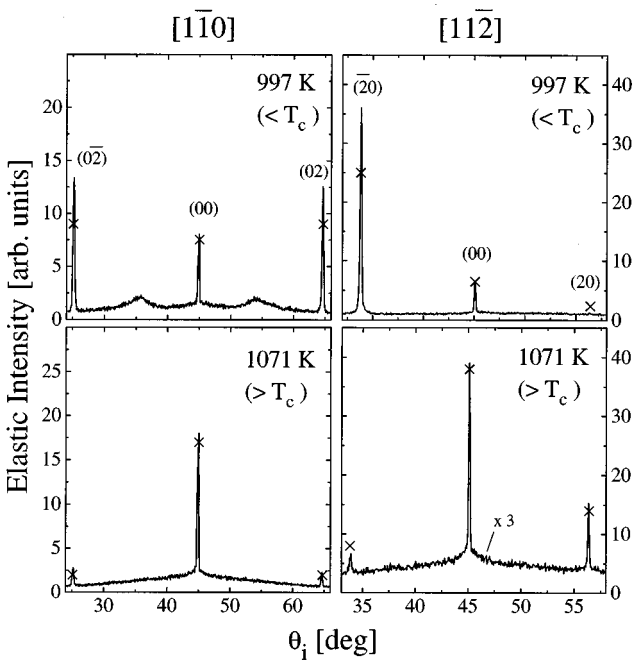


FIG. 11. Angular distributions of He scattered from Ge(111) at temperatures below and above $T_c = 1050$ K. Incident He energy 22 meV ($\lambda = 0.95$ Å). The crosses indicate the best-fit peak intensities (see the text for details).

### C. The order-order transition at $T_c = 1050$ K

Having gained some knowledge on the reliability of the HCW approach in the case of the $c(2\times8)$ structure, we have addressed the question of performing a similar analysis of the $1\times1$ structures present above and below the order-order transition that takes place on Ge(111) at $T_c = 1050$ K. As recently reported,[10] the presence of sharp integral-order peaks that change only their relative amplitudes at $T_c = 1050$ K indicates the persistence of long-range $1\times1$ order in the first bilayer well above $T_c$. Angular distributions along [110] and [112] measured at temperatures above and below $T_c$ are illustrated in Fig. 11. Note the asymmetry reversal observed along [11$\bar{2}$] for $T > T_c$. The fact that the fractional-order beams disappear at lower temperatures along [112] than along [110] indicates that delocalization of the adatoms proceeds via correlated diffusion along [110], as recently suggested on the basis of *ab initio* calculations.[18] For increasing temperature, the diffraction peaks show the usual Debye-Waller exponential decrease due to thermal attenuation. This can be seen in Fig. 12, where the intensities of some integer-order peaks along [112] are shown as a function of temperature. For a full description of the experimental findings related to the order-order transition the reader is referred to Ref. 10.

In order to perform intensity calculations with the eikonal approximation, elastic intensities for the two $1\times1$ stuctures have been normalized to $T_c = 1050$ K. The intensities obtained in this way for different He wavelengths are listed in Table III (for $T < T_c$) and Table IV (for $T > T_c$). In a first step, the calculations were performed by choosing a Fourier representation for the corrugation function, as the one given by Eq. (1). For $T < T_c$, best agreement with the experiment was achieved with $D = 4$ meV, $a(02) = a(11) = 0.45$ Å, and $b(02) = -b(11) = 0.28$ Å. For the structure present at

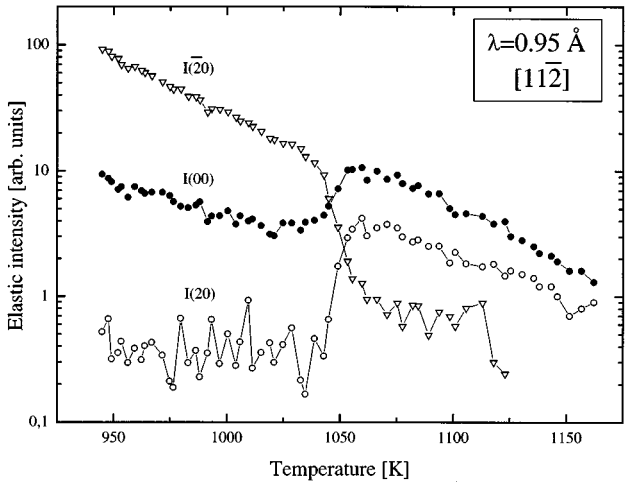


FIG. 12. Temperature dependence of areas measured for the specular and some integer-order diffraction peaks for He scattered elastically from Ge(111) along [11$\bar{2}$].

$T > T_c$, the best-fit parameters are $a(02) = a(11) = 0.07$ Å, $b(02) = -b(11) = 0.27$ Å, and $D = 4$ meV. As in the case of the $c(2\times8)$ reconstruction, the fits can be sligtly improved by modeling the corrugation function by Gaussian hills. This was made by considering first- and second-layer atoms as independent groups of hills $G(x,y)$ of amplitudes $h_1$ and $h_2$, respectively. The hills were assumed to be symmetric, i.e., $\sigma_1 = \sigma_{1_x} = \sigma_{1_y}$ and $\sigma_2 = \sigma_{2_x} = \sigma_{2_y}$. The atoms were fixed at their theoretical bulk positions, i.e., at $(x_i, y_i) = (0,0)$, $(0, a_2)$, $(a_1, 0)$, $(a_1, a_2)$, and $(\frac{1}{2}a_1, \frac{1}{2}a_2)$ for first-layer atoms and $(x_i, y_i) = (0, \frac{1}{3}a_2)$, $(a_1, \frac{1}{3}a_2)$, and $(\frac{1}{2}a_1, \frac{10}{12}a_2)$ for second-layer atoms. The best-fit parameters corresponding to $\lambda = 0.95$ Å, and $D = 4$ meV are $h_1 = 0.70$ Å, $h_2 = 0.53$ Å, and $\sigma_1 = 2.0$ for $T < T_c$ and $h_1 = 0.25$ Å, $h_2 = 0.40$ Å, and $\sigma_1 = 2.0$ for $T > T_c$. The intensities calculated with this wavelength for both $1\times1$ structures are compared in Tables III and IV to the experimental data. Also shown are the intensities calculated for $\lambda = 0.81$ Å and $\lambda = 1.14$ Å using the best-fit parameters derived for $\lambda = 0.95$ Å. Very good agreement is achieved also in this case except for the (20) beam at $T < T_c$ and $\lambda = 0.81$ Å. This intensity could not be reproduced at all even by allowing the parameters to vary; the origin of this discrepancy is not clear at the moment. Gray scale representations of both corrugations are displayed in Fig. 13. Note that $+\zeta(x,y)$ looks very similar to $-\zeta(-x,-y)$ in both surfaces, which means that we do not have to care about which of the two possible corrugations is the correct one. The maximum corrugation amplitudes at $T < T_c$ along [110] and [112] are $\zeta_X \sim 0.60$ Å and $\zeta_Y \sim 0.95$ Å, respectively. These values represent $\sim 15\%$ of the corresponding lattice constant, making a comparison with exact HCW calculations necessary. Calculations performed with use of the $RR'$ method indicate that the problem is within the range of convergence of the eikonal approximation; the corresponding intensities are also shown in Tables III and IV. As expected from its smaller corrugation amplitude, the agreement is much better for the $1\times1$ structure at $T > T_c$. The importance of modeling the surface corrugation with different mathematical functions can be seen more clearly in the results corresponding to $T < T_c$. The intensity of the (02)

TABLE III. Best-fit intensities calculated with the eikonal approximation and the $RR'$ method for the $1\times1$ structure at $T<T_c$. Results derived by modeling the surface with a Fourier ansatz and with Gaussian hills are listed in both cases. All calculations were performed with $D=4$ meV (see the text for further details).

| λ (Å) | Azimuth | $\theta_i$ (deg) | Beam | $I_{\text{expt}}$ | $I_{\text{eiko}}^{\text{Gauss}}$ | $I_{RR'}^{\text{Gauss}}$ | $I_{\text{eiko}}^{\text{Fourier}}$ | $I_{RR'}^{\text{Fourier}}$ |
|---|---|---|---|---|---|---|---|---|
| 0.95 | $[\bar{1}10]$ | 45.0 | (00) | 1.00 | 1.00 | 1.00 | 1.00 | 1.00 |
| | | 64.7 | ($0\underline{2}$) | 1.88 | 1.96 | 1.43 | 0.64 | 0.50 |
| | | 25.4 | (02) | 2.36 | 1.99 | 1.45 | 0.70 | 0.53 |
| 0.95 | $[11\bar{2}]$ | 45.0 | (00) | 1.00 | 1.00 | 1.00 | 1.00 | 1.00 |
| | | 56.3 | ($\underline{2}0$) | 0.09 | 0.55 | 0.58 | 0.06 | 0.00 |
| | | 33.8 | ($\bar{2}0$) | 3.40 | 3.60 | 3.54 | 3.43 | 2.70 |
| | | 67.9 | ($\underline{4}0$) | 0.81 | 0.34 | 0.23 | 0.12 | 0.03 |
| | | 22.1 | ($\bar{4}0$) | 0.63 | 0.91 | 0.66 | 1.55 | 1.05 |
| 1.14 | $[11\bar{2}]$ | 45.0 | (00) | 1.00 | 1.00 | 1.00 | 1.00 | 1.00 |
| | | 58.6 | ($\underline{2}0$) | 0.05 | 0.30 | 0.24 | 0.01 | 0.04 |
| | | 31.6 | ($\bar{2}0$) | 1.60 | 1.80 | 1.25 | 1.80 | 1.26 |
| 0.81 | $[11\bar{2}]$ | 45.0 | (00) | 1.00 | 1.00 | 1.00 | 1.00 | 1.00 |
| | | 54.5 | ($\underline{2}0$) | 0.38 | 0.69 | 1.39 | 0.77 | 0.48 |
| | | 35.6 | ($\bar{2}0$) | 0.70 | 3.69 | 7.01 | 5.90 | 7.14 |

and $(0\bar{2})$ beams, for example, cannot be reproduced at all with a Fourier ansatz, whereas very good agreement is achieved by modeling the structure with Gaussian hills.

A look into the best-fit models shown in Fig. 13 reveals that in addition to a decrease of the total corrugation amplitude, the phase transition is characterized by a symmetry reversal of the top layer by 180°. It must be mentioned that the question about which of the corrugations correspond to the normal bulk truncated surface can be unambiguously answered by comparing them to the ones obtained for the $c(2\times8)$ reconstruction. As a consequence, our results show that important structural changes take place at $T_c$, in that the first-layer atoms are shifted from their original bulk positions to sites in the hexagonal diamond lattice. This is in agreement with recent first-principles molecular-dynamics calculations performed by Selloni *et al.*,[18] where the first layer was found to occupy both regular and hexagonal diamond sites but with a small excess in favor of the hexagonal sites. Due to repulsion of similar atoms placed in the fourth layer an outward protusion is observed, which is responsible for the symmetry reversal observed at $T>T_c$. This contrasts with the general picture presented in Ref. 10, after which the behavior of the diffraction peaks across $T_c$ could be explained by a shrinkage of the top bilayer of about 10%. Our simulations show clearly that the asymmetry reversal observed along $[112]$ for $T>T_c$ actually reflects the ocurrence

TABLE IV. Best-fit intensities calculated with the eikonal approximation and the $RR'$ method for the $1\times1$ structure at $T>T_c$. Results derived by modeling the surface with a Fourier ansatz and with Gaussian hills are listed in both cases. All calculations were performed with $D=4$ meV (see the text for further details).

| λ (Å) | Azimuth | $\theta_i$ (deg) | Beam | $I_{\text{expt}}$ | $I_{\text{eiko}}^{\text{Gauss}}$ | $I_{RR'}^{\text{Gauss}}$ | $I_{\text{eiko}}^{\text{Fourier}}$ | $I_{RR'}^{\text{Fourier}}$ |
|---|---|---|---|---|---|---|---|---|
| 0.95 | $[\bar{1}10]$ | 45.0 | (00) | 1.00 | 1.00 | 1.00 | 1.00 | 1.00 |
| | | 64.7 | ($0\underline{2}$) | 0.10 | 0.04 | 0.01 | 0.02 | 0.03 |
| | | 25.4 | (02) | 0.14 | 0.05 | 0.02 | 0.03 | 0.04 |
| 0.95 | $[11\bar{2}]$ | 45.0 | (00) | 1.00 | 1.00 | 1.00 | 1.00 | 1.00 |
| | | 56.3 | ($\underline{2}0$) | 0.33 | 0.30 | 0.24 | 0.27 | 0.29 |
| | | 33.8 | ($\bar{2}0$) | 0.07 | 0.10 | 0.07 | 0.09 | 0.08 |
| | | 67.9 | ($\underline{4}0$) | 0.00 | 0.02 | 0.00 | 0.02 | 0.02 |
| | | 22.1 | ($\bar{4}0$) | 0.00 | 0.00 | 0.00 | 0.00 | 0.00 |
| 1.14 | $[11\bar{2}]$ | 45.0 | (00) | 1.00 | 1.00 | 1.00 | 1.00 | 1.00 |
| | | 58.6 | ($\underline{2}0$) | 0.16 | 0.20 | 0.13 | 0.20 | 0.18 |
| | | 31.6 | ($\bar{2}0$) | 0.03 | 0.08 | 0.06 | 0.07 | 0.06 |
| 0.81 | $[11\bar{2}]$ | 45.0 | (00) | 1.00 | 1.00 | 1.00 | 1.00 | 1.00 |
| | | 54.5 | ($\underline{2}0$) | 0.38 | 0.46 | 0.37 | 0.41 | 0.45 |
| | | 35.6 | ($\bar{2}0$) | 0.08 | 0.12 | 0.10 | 0.11 | 0.10 |

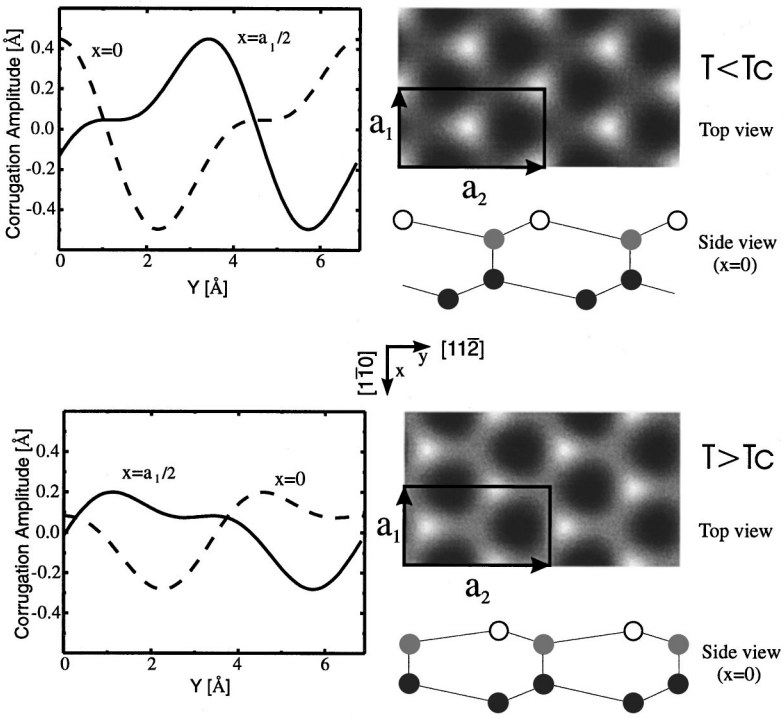


FIG. 13. Gray scale representation of the best-fit corrugations obtained for both ordered $1\times1$ structures at $T<T_c$ and $T>T_c$. The corresponding cuts along [112] are displayed on the left. The sphere models represent side views at $x=0$.

of a similar reversal in the structure of the surface, which cannot be reproduced by a simple reduction of the top bilayer spacing.

## IV. CONCLUSION

Our He-scattering investigations of the Ge(111)–$c(2\times8)$ reconstruction demonstrate the existence of a buckling between the two rest atoms within the unit cell, constituting experimental support of the STM measurements reported by Hirschorn *et al.*[8] The question about possible links between the HCW approximation and the existence of buckling was examined by performing calculations with the close-coupled-channel method with a realistic potential. The results provide a ''range of confidence'' for conclusions based on the HCW assumption, which are fullfiled in the particular case of the $c(2\times8)$ reconstruction. To our knowledge, this is the first time that such an analysis has been carried out for a highly corrugated two-dimensional system. A similar analysis of spectra measured above and below the order-order transition at $T_c=1050$ K reveals that important structural changes of the topmost layer occur for $T>T_c$, in which the first-layer atoms are shifted from their regular bulk places to the hexagonal diamond sites, as suggested recently by Selloni *et al.*[18] on the basis of *ab initio* calculations. This contrasts with the explanation given in Ref. 10, after which the intensity changes observed at $T>T_c$ are caused by a reduction of the top bilayer spacing of 10%. This possibility can be clearly ruled out on the basis of our analyses. In summary, we have shown that despite the large unit cells, the appreciable two-dimensional corrugation amplitude, and the complexity added by the presence of three domains in the case of the $c(2\times8)$ reconstruction, calculations performed within the simple HCW model reveal all the structural details of the surface. We hope that these results will stimulate new structure determinations of reconstructed semiconductor surfaces by means of He diffraction.

[1] P. W. Palmberg and W. T. Peria, Surf. Sci. **6**, 57 (1967).
[2] D. J. Chadi and C. Chiang, Phys. Rev. B **23**, 1843 (1981).
[3] W. S. Yang and F. Jona, Phys. Rev. B **29,** 899 (1984).
[4] R. J. Phaneuf and M. B. Webb, Surf. Sci. **164**, 167 (1985).
[5] R. S. Becker, J. A. Golovchenko, and B. S. Swartzentruber, Phys. Rev. Lett. **54**, 2678 (1985).
[6] R. S. Becker, B. S. Swartzentruber, J. S. Vickers, and T. Klitsner, Phys. Rev. B **39**, 1633 (1989).
[7] P. Molinàs-Mata and J. Zegenhagen, Surf. Sci. **281**, 10 (1993).
[8] E. S. Hirschorn, D. S. Lin, F. M. Leibsle, A. Samsavar, and T.-C. Chiang, Phys. Rev. B **44**, 1403 (1991).
[9] N. Takeuchi, A. Selloni, and E. Tosatti, Phys. Rev. Lett. **69**, 648 (1992).
[10] C. A. Meli, E. F. Greene, G. Lange, and J. P. Toennies, Phys. Rev. Lett. **74**, 2054 (1995).
[11] J. P. Toennies, in *Surface Phonons*, edited by W. Kress and F. W. de Wette (Springer, Berlin, 1991).
[12] G. Brusdeylins, R. B. Doak, and J. P. Toennies, Phys. Rev. B **27**, 3662 (1983).
[13] J. P. Toennies and R. Vollmer, Phys. Rev. B **44**, 9833 (1991).
[14] Virginia Semiconductor Inc., 1501 Powhatan St., Fredicksburg, VA 22401.
[15] U. Garibaldi, A. C. Levi, R. Spadacini, and G. E. Tomei, Surf. Sci. **48**, 649 (1975).
[16] N. García and N. Cabrera, Phys. Rev. B **18**, 576 (1978).
[17] N. Cabrera, V. Celli, F. O. Goodman, and R. Manson, Surf. Sci. **19**, 67 (1970); R. J. Blake, Comput. Phys. Commun. **33**, 425 (1984).
[18] A. Selloni, N. Takeuchi, and E. Tosatti, Surf. Sci. **331-333**, 995 (1995).